Author Accepted Manuscript (AAM)

Analytical and experimental study of high velocity impact on ceramic/nanocomposite targets

H. Shanazari [1], GH. Liaghat [1,2 *], S. Feli [3], H. Hadavinia [2]

[1]Department of Mechanical Engineering, Tarbiat Modares University, Tehran, Iran

[2]School of Mech & Auto Engineering, Kingston University London, SW15 3DW, UK

[3]Department of Mechanical Engineering, Razi University, Kermanshah, Iran

Abstract

In this paper, an analytical model has been developed for modeling high velocity impact on ceramic/nanocomposite targets. In this model penetration resistance of ceramic is determined based on cavity expansion analysis and variables during perforation of projectile onto ceramic are considered. Also semi-angle of ceramic conoid is modified. This angle depends on impact velocity and changes during perforation process. For modeling the back-up composite laminate, the kinetic and strain energy of yarns and shear plugging have been determined. A failure model based on the energy absorption until failure of laminate composite is used. Ballistic impact tests were performed to validate the analytical predictions. These tests were performed by firing 10 mm steel flat ended projectile onto ceramic/composite target. Front layer is alumina ceramic and composite laminates of back up made of E-glass/epoxy with and without nano zirconia particle of 5 wt%. The effect of nano zirconia dispersion in the matrix for different failure modes is discussed. Experimental results revealed an improvement in the ballistic performance of samples with nano zirconia particle. The analytical predictions of ballistic limit velocity and residual velocity of projectile are found to be in good agreement with the experimental results.

Keywords

Ceramic, nanocomposite, analytical model, high velocity impact

Introduction

Ceramic materials are widely used in armor systems as well as aircraft structures and military vehicles for the advantages of low density, high compressive strength, hardness, and heat resistance. By supporting the ceramic facing with a ductile material, the ballistic performance of the armors can be dramatically increased. Ceramics and composite combinations have clear advantages as an armor material compared with the other armor materials such as rigid metal armor. Ceramics/composite materials are widely used in military vehicles such as tanks because of their high bulletproof performance. The utilization of composite materials armor in certain ballistic applications is increasingly preferred over conventional metal armor systems because of its superior strength-to-weight ratio. [1] It is important to understand the

* Corresponding author: GH Liaghat, Department of Mechanical Engineering, Tarbiat Modares University, P.O. Box 14115-141, Tehran 55555, Iran. Email: ghlia530@modares.ac.ir

energy absorption and damage mechanisms of such armor systems for predicting their behavior under ballistic impact. In the impact process on ceramics, the ceramic destroys the projectile tip, slows it down, and distributes the load over a large area of the back-up material. The back-up plate supports the ceramic and brings the comminuted ceramic and projectile to rest. The back-up plate material is selected on the basis of structural, ballistic, and weight considerations. Kevlar, fiberglass, and metals such as aluminum are most commonly used as the backing material.

Even though there are numerous studies on the ballistic impact behavior of composite, ceramic, and ceramic/metal targets, [2–4] only few studies report on the ballistic impact performance of the ceramic/composite armors. In Florence's model, [5] a global energy balance is proposed, leading to the derivation of the ballistic speed limit. The Woodward model [6] investigates penetration mechanisms considering the lumped mass approach. This model presents analytical solutions for the calculation of velocity and residual mass of a projectile at any instant of time after impact. In 1998, Chocron and Sanchez-Galvez [7] presented a model where the back plate of the armor is made of polymer composite material.

The model allows the calculation of residual velocity, residual mass, the projectile velocity, and the deflection and strain histories of the back-up plate. Zeara and Sachez-Galvez [8] presented an analytical model to simulate ballistic impact of projectiles on ceramic/metal armors based on the work presented by Tate [9] for projectile penetration into ceramic and by Woodward6 for the behavior of metal backing plate. Naik et al. [10] developed an analytical model to simulate the ballistic impact behavior of ceramic/composite armors. The model is based on wave theory and energy balance between the kinetic energy of the projectile and the energy absorbed by different mechanisms. Liaghat et al. [11] developed an analytical model based on the Woodward model and lumped mass method which predicts ballistic behavior of ceramic armors. Feli and colleagues [12,13] developed a numerical and analytical model for the perforation of ceramic/multi-layer woven fabric and ceramic/composite targets by blunt projectiles. Residual velocity, velocity–time history, residual mass of fragmented ceramic conoid, penetration depth, and energy absorbed by woven fabric are all estimated by this analytical model. Velocity–time history of the projectile shows a good agreement with the Chocron–Galvez numerical model. Liu et al. [14] studied the influence of different back laminate layers (Ti6Al4V/UHMWPE/Ti6Al4V) on the ballistic performance of ceramic composite armor around the experiments and numerical simulation. Krishnan et al. [15] discuss a numerical modeling of ceramic composite armor systems with a backing made of ultra-high-molecular-weight polyethylene (UHMWPE). Experimental results show that the finite element predictions of damage are excellent though the back face deformations are under predicted. Cheeseman and Bogetti [16] present a review of the factors that influence the ballistic performance; specifically, the material properties of the yarn, fabric structure, projectile geometry and velocity, far field boundary conditions, multiple plies, and friction.

There are many experimental and analytical studies on the ballistic impact behavior of laminated composite materials. Talib et al. [17] studied the impact performance of a hybrid composite made of woven fiber Kevlar-29 and Al2O3 powder/epoxy subjected to high-velocity impact. In the study carried out by Shaktivesh et al., [18] the ballistic impact performance of structures made of polymer matrix composites has been investigated. The method used in the study considers both shear plugging and tensile failure during conical deformation on the back face of the target. Naik et al. [19] studied the ballistic impact

behavior of typical woven fabric E-glass/epoxy composites. This analytical method is based on wave theory. Wen et al. [20] developed analytical equations for predicting the penetration and perforation of FRP laminates struck at normal incidence over a wide range of impact velocity. Ceramic damage is studied by quantifying the size and distribution of fragments in the recovered sample. Mohan and Velu [21] developed a modified analytical model, based on Naik model, to predict the impact behavior of unidirectional cross ply laminates. This model can predict the energy absorbed by different damage and energy absorbing mechanisms. Chen et al. [22] developed a modified analytical model based on the momentum theory, taking into account the strain gradient between the panel layers and its effects on the tensile strain at the edge of the projectile. Shanazari et al. [23] developed a new analytical model for the prediction of the ballistic behavior of hybrid composite panels. This model analyzes penetration process of projectile onto hybrid composite panels (consisting of UD and woven fabric) based on wave propagation and energy balance for the ballistic protection.

In the present study, an analytical model is developed for the prediction of the ballistic impact behavior of ceramic/composite armors. In this model, the penetration resistance of the ceramic has been determined based on the cavity expansion analysis and variations during perforation of projectile on ceramic have been considered. Also angle of the ceramic conoid is modified. This angle depends on the impact velocity and changes during the perforation process. The effect of nano-zirconia dispersion in the matrix (in the composite back up material) is discussed for different failure modes.

Analytical model

When a projectile with the high kinetic energy impacts on a ceramic tile, a shattered zone in a form of conoid will be formed. Damages occurred in ceramic tiles are mainly in the forms of tensile failure, shear plugging, cracking and pulverization. The armor of ceramic/composite material is made of two different materials having different properties. The ceramic material receives the initial impact of the projectile which leads to destruction of the head of the projectile progressively as it penetrates to the composite layers. In the first stage a major part of the impact energy is dissipated. Then in the second stage the back-up ductile material absorbs the residual impact energy caused by the fragmented parts of the projectile as it perforates the material. Description of each stage is presented in the following sections.

First stage

In the first stage, the destruction of the head of the projectile before penetration into the ceramic layer plus the formation of cone cracks occurs. During this stage, the impact of the projectile generates compressive shock waves which travel across the ceramic thickness. This wave will reflect back as a tension wave which tends to crack the ceramic and cause the fractured cone formation. It is assumed that the time taken to form this cone is equal to $t = 6(h/c)$, [24] where h is the thickness of the ceramic plate, and c is the longitudinal velocity of the sound. During the formation of the cone, the projectile is being eroded, but the ceramic does not move at all. The part of the projectile that is being eroded is called the plastic part, and in this phase, its penetration velocity is zero. The rear of the projectile moves at a velocity v(t). This velocity and mass of projectile are governed by Tate's equations [5]

$$\mathrm{M_p}\frac{\mathrm{dv}}{\mathrm{dt}} = -\mathrm{Y_p}.\mathrm{A_p} \quad \text{and} \quad \frac{\mathrm{dM_p}}{dt} = \rho_p A_p v \tag{1}$$

Second stage

The second stage starts at $t = 6(h/c)$ and now the whole armor contributes to reducing the impact energy (Figure 1). The rear part of the projectile moves at a speed v(t), the ceramic-projectile interface at $\dot{x}(t)$ and the cone at $\dot{u}_0(t)$. In this region, the pressure in the projectile–ceramic interface is much higher than the yielding stress of the involved materials.

Projectile equations. In a normal impact, depending on the velocity of the ceramic-projectile interface, the tip of the projectile will be either eroding or not.

Erosion of projectile $\dot{x} < v$. In this phase Tate's equation [5] is written as follows

$$\mathrm{Y_p} + \frac{1}{2}\rho_p(v - \dot{x})^2 = R_t + \frac{1}{2}\rho_c(\dot{x} - \dot{u}_0)^2 \qquad (2)$$

where R_t is the dynamic resistance strength against penetration into the ceramic. However, the reduction in the weight of the projectile is given by the following

$$\frac{\mathrm{dM_p}}{dt} = \rho_p A_p(v - \dot{x}) \qquad (3)$$

Modification of penetration resistance of ceramic. In this paper, based on the cavity expansion analysis, the analytical model for the determination of the penetration resistance of ceramic is improved. The cavity expansion analysis was initially used to study ductile materials (such as metals) on which no cracked area occurs easily. [25] However, for brittle materials like ceramics, damage exists in radially cracked region. According to the study by Satapathy and Bless, [26] the response region in ceramic due to sudden cavity expansion include of five zones (Figure 1): cavity, comminuted, radially cracked zone, elastic zone, and undisturbed zone which radial distances of them are $r = h, a, c, b$, respectively. As the cavity is subjected to an instantaneous expansion velocity, an elastic wave spreads in the ceramic. At the elastic-undisturbed interface, there is no stress. The hoop stresses in the elastic region are tensile. Since the tensile strength of the material is very low, radial cracks appear when the hoop stresses equal the tensile strength. The material in the cracked zone can support only compressive radial stress. When the radial stress in cracked zone reaches to the compressive strength of the material, the cracked material will be crushed more and is reduced to a powder (comminuted). By calculating the radial and hoop stress in these regimes, the ceramic penetration resistance in finite and infinite targets can be determined. In finite targets, for a given geometry (h and b known), equation (4) can be obtained as follows [26]

$$\frac{1}{3}\left(\frac{h}{a}\right)^3 = \frac{\sigma_f}{2E_c\left(1+\frac{1b^3}{2c^3}\right)}\left[\frac{(1-2\vartheta)c^3+(1+\vartheta)b^3}{c^2 a}\right] + \frac{Y}{E_c}\left(1 - \frac{a}{c}\right) \qquad (4)$$

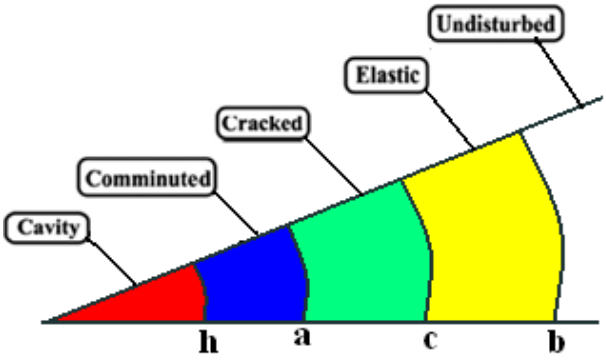

Figure 1. Response regions in the ceramic targets [25].

And then the target dynamic resistance strength is defined as

$$R_t = Y(a/h)^{2\alpha}, \quad and \quad \alpha = 6\gamma/(3+4\gamma) \tag{5}$$

Where γ is the pressure-shear coefficient.

For an infinite target (i.e. when b is very large), the R_t is only a function of c and it can be evaluated as described in [15]:

$$R_t = Y\left[\frac{\frac{E}{3Y}}{1-\sqrt{\frac{\sigma_f}{Y}}\frac{(1-\vartheta)}{\sqrt{2}}}\right]^{2\alpha/3} \tag{6}$$

Then, the penetration resistance of the ceramic at the initial impact is defined, and variation of this parameter during penetration process can be determined as follows [21]

$$R_t' = R_t\left(\frac{\dot{x}-\dot{u}_0}{\dot{x}_1}\right)^2 \tag{7}$$

where $\dot{x}$ is the penetration velocity at the end of the first phase, and R_t is the penetration resistance of the ceramic at the initial impact.

Rigid projectile $\dot{\mathbf{x}} = \mathbf{v}$. During penetration it is possible that the velocity of the projectile is equal to the projectile–ceramic interface velocity which means the projectile is not eroding further and the mass is maintained constant. The residual mass of the projectile M_{pr} continues to penetrate the completely fractured ceramic. The force acting by the comminuted ceramic is given by

$$M_{\mathrm{pr}}\frac{\mathrm{dv}}{\mathrm{dt}} = -R_t.A_p \tag{8}$$

Ceramic equation

The governing equation of the motion of the ceramic cone considering the mass of ceramic conoid is time dependent and it is written as

$$\frac{d(M_c\dot{u}_0)}{dt} = 2Fcos\theta + R_tA_p \tag{9}$$

where M_c is the mass of the ceramic cone.

Modified ceramic conoid angle. The ceramic conoid semi-angle is an important parameter. There are different estimate for this angle. [6,27,28] For example, Woodward [6] considered this angle about 68° (the angle formed in quasi-static state). This is according to different approaches and considering the fact that in high-impact velocities, because of high energy of projectile, the projectile–ceramic interface force is more than the ceramic erosion stress. Therefore, the erosion of ceramic and then the penetration of projectile into ceramic will occur.

When erosion of ceramic occurs, the effective dimensions of the ceramic conoid are reducing. In fact, when ceramic erodes, new ceramic conoids with smaller dimensions will be formed. The higher impact velocity results in smaller ceramic conoid. The semi-angle of ceramic can be approximated by equation (10). [23] In this equation, this angle changes linearly between 68° in Woodward model [6] and 63° in Florence model [5]

$$\varphi = \begin{cases} 68 & V_P < 600 \\ \frac{\pi}{180}\left[\frac{1}{60}(-V_P + 900) + 63\right] & 600 < V_P < 900 \\ 63 & V_P > 900 \end{cases} \quad (10)$$

i.e. for impact velocities less than 600 m/s, the semiangle φ is equal 68° and for velocities more than 900 m/s, it is 63° and between them, changes linearly according to equation (9). Zaera and Sanches-Galvez [8] showed that by increasing the impact velocity, the failure part increases and the dimensions of the cone decrease.

On the other hand, the semi-angle of the conoid is considered variable during penetration process, and it is assumed that sides of newly formed cone are not parallel to the original cone and the effective dimensions of the ceramic cone decrease (Figure 2). The change of the angle approximately can be found form

$$\varphi = \frac{\pi}{180}\left[\frac{\varphi_0 - 34}{t_c}(t_c - x) + 34\right] \quad (11)$$

where x is ceramic eroded length, t_c is the thickness of ceramic and φ_0 is the semi-angle of initial cone determined by equation (9).

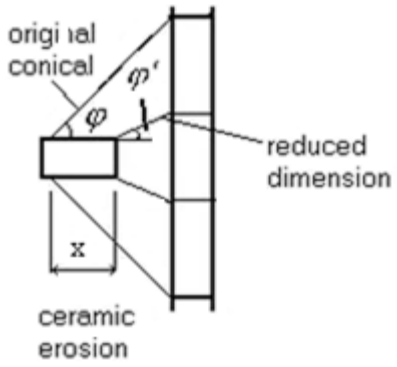

Figure 2. Reducing the semi-angle ceramic cone in an impact.

In other words

– In case there is no ceramic erosion, the angle φ is at its maximum value.

– In case of highest possible erosion (total ceramic thickness), the angle φ is 34° (minimum value in Fellows and Bartan model [29]).

In summary, the angle of a newly formed ceramic cone with semi-angle φ_0 is determined by equation (10), and the angle will change during perforation according to equation (11).

In the present analysis, two stages are considered for the penetration process into laminated composite backup plate of the ceramic. In the first stage, called the shearing and compression stage, Figure 3(a), a compressive stress wave created after the impact continues to propagate in the through-thickness direction as the projectile penetrates further. In fact, a considerable compressive force is generated between the projectile and the laminate, as the fiber layers in the contact zone are compressed. Meanwhile, a shearing force is generated at the edge of the contact zone as a result of the substantial velocity gradient between the contact zone and the harmonious deformation zone.

The second stage, called the stretching deformation stage (Figure 3(b) and (c)), starts when the tension stress wave reaches the contact surface and a considerable stretching deformation occurs in the non-perforated fiber layers. During this stage, the dynamic transient response of the laminate is mainly considered. At the beginning of this stage, the fiber layers that did not fail create a dynamic cone form. Residual kinetic energy of the projectile is mainly absorbed by stretching deformation of the unsheared fiber layers, the deformation cone, and through the delamination and matrix cracking in the transition layers. During the propagation process of the compressive stress wave, the dynamic compressive force F_{1C} applied on the projectile can be written as [30]

$$\mathrm{F_{1c}} = \sigma_{cd} A_c = \left(1 + \beta\sqrt{\rho_t/\sigma_c}\,\dot{u}_0\right) A_c \sigma_c \tag{12}$$

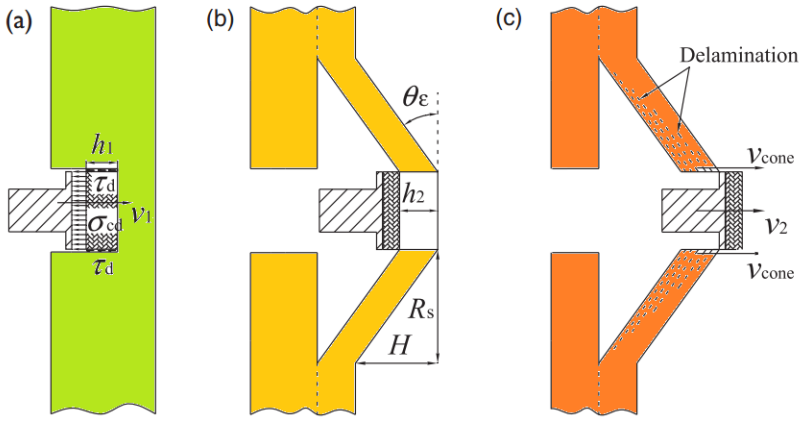

Figure 3. Schematics of the stages of the perforation process. (a) first stage: shearing and compression; (b) second stage: stretching deformation; and (c) end of the second stage.

Hence, the dynamic compressive stress, σ_{cd} is defined according to Wen [20], where β is a shape factor related to the nose shape of the projectile (for projectiles with a blunt nose, $\beta = 1$), σ_c is the quasi-static compressive strength in the through-thickness direction of the

laminate and $\dot{u}_0$ is the instantaneous velocity of the ceramic-composite interface. It is assumed that shear stress decrease linearly through the laminate thickness. Thus, the shearing force acting on the projectile is given by

$$F_{1s} = \pi d_c \tau_d [h_t - x_1]/2 \quad 0 \le x_1 \le h_t \,,\ where \ \ \tau_d = \tau_s + \mu\dot{\gamma} \tag{13}$$

where h_t is the total thickness of the laminate, x_1 is the penetration distance of the projectile, τ_d is the dynamic shear strength of the laminate, τ_s is the quasi-static shear strength of laminate, μ is the viscosity coefficient, and $\dot{\gamma}$ is the shear strain rate.

The inertial force during the propagation of the compressive stress wave is obtained as follows

$$F_{1i} = \rho_t C_t A_c \dot{u}_0/8 = \pi d_c^2 \rho_t c_t \dot{u}_0/32 \tag{14}$$

where C_t is the velocity of the compressive stress wave in the thickness direction. Thus, total force can be obtained by

$$F_1 = F_{1c} + F_{1s} + F_{1i} \tag{15}$$

In the second stage, during the formation and movement of the deformation cone, the kinetic energy of the projectile is mainly absorbed by elastic deformation mechanism and moving of the deformation cone. By considering the average velocity in the contact zone of the deformation cone, the inertial force F_{2i} that acts on the projectile during the formation and movement of the deformation cone is obtained by

$$F_{2i} = \rho_t A_c \dot{u}_0^2/8 = \frac{\pi \rho_t d_c^2 \dot{u}_0^2}{32} \tag{16}$$

The tensile force that acts on the projectile F_{2L} is the transverse component of the tensile stresses in the unsheared fiber layers

$$F_{2L} = \pi d_c h_2 \sigma_\varepsilon \tag{17}$$

where h_2 is the total thickness of the unsheared fiber layers, h_2=h_t-h_1 and $\sigma_\varepsilon = E\varepsilon$ is the dynamic tensile strength of the laminate. Thus, total force can be obtained by

$$F_2 = F_{2i} + F_{2L} \tag{18}$$

The relation between $\dot{u}_0$ and the strain of yarns based on the Smith et al. [31]

$$\dot{u}_0 = c_y \sqrt{\varepsilon[2\sqrt{\varepsilon(\varepsilon+1)} - \varepsilon]} \tag{19}$$

Here, c_y is the longitudinal wave speed in the yarn. The angle between the line of impact and the yarn is given by

$$\sin\theta = \frac{\sqrt{\varepsilon\left[2\sqrt{\varepsilon(\varepsilon+1)}-\varepsilon\right]}}{\sqrt{\varepsilon(1+\varepsilon)}} \tag{20}$$

Effects of strain rate on yarns. In this paper, glass fiber is used for planar woven fabrics as a back-up plate material. Figure 4 shows the stress–strain curves of glass fiber under different loading conditions. [32] By considering high-velocity impact of projectile, the equations are used for the approximation of stress–strain relation of glass fiber at about 1000/s strain rate. Because E increases significantly with increasing strain rate, it is obviously not reasonable if we introduce the Young's modulus E at quasi-state to the analytical model.

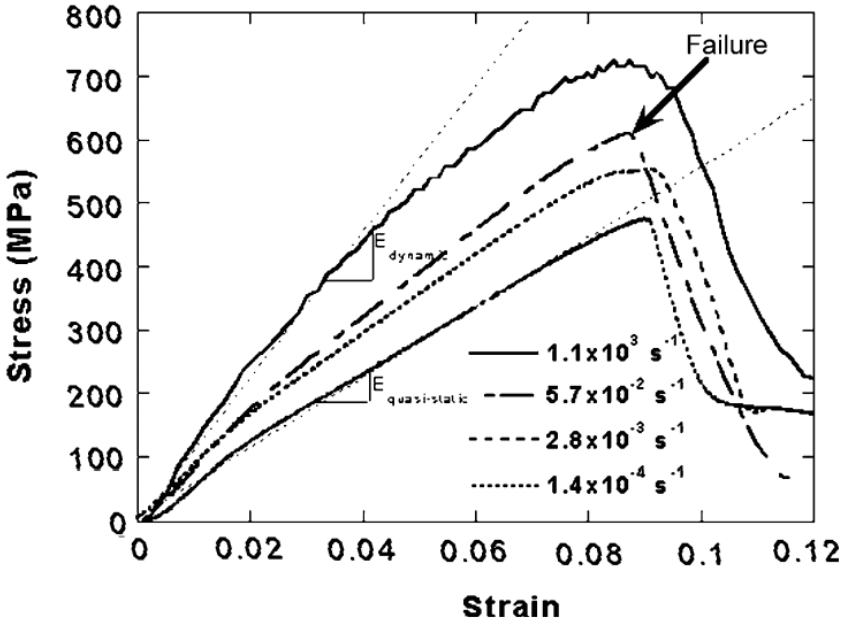

Figure 4. Stress/strain curves of the composite at different strain rates [32]

Failure of composite laminate. In this analytical model, the total strain and kinetic energy and shear plugging absorbed until failure by the back-up is used to calculate the instant of failure. When the strain in yarns becomes greater than failure strain, it fails. The tensile failure energy of primary yarns (yarns directly below the projectile) is given by:

$$E_{pri} = A\int_0^x \int_0^{\varepsilon} \sigma(\varepsilon) d\varepsilon dx = E.\varepsilon_{pri}^2.2D_p.d_y.A.\mathrm{r_l(t)} \quad (21)$$

where ε_{pri} is strain in the primary yarn, dy is density of yarns in weft and warp directions, A cross section area of a yarn and r_1 is radial distance of longitudinal wave.

The secondary yarns (all the yarns in each layer other than the primary yarns) experience different strains depending on their position. The energy absorbed in the deformation of all the secondary yarns can be obtained by the following equation [9]:

$$E_{sec} = \int_{D_{p/2}}^{r_t(t)} \left(\int_0^{\varepsilon_{sec}(t)} \sigma(\varepsilon_{sec}) d\varepsilon_{sec}\right).h.\left\{2\pi r - 8r\sin^{-1}\left(\frac{D_p}{2r}\right)\right\} dr \quad (22)$$

where ε_{sec} is strain of secondary yarn and equal to $\varepsilon_{sec}(t) = \frac{\mathrm{r-D_p/\sqrt{2}}}{r_t(\mathrm{t})-\mathrm{D_p}/\sqrt{2}}\varepsilon_{pri}(\mathrm{t})$,and r_t is radial distance traveled by transverse wave. The cone formed on the back face of the target absorbs some energy. Mass and energy of the cone formed are, respectively

$$M_C = \pi r_t^2 h\rho \quad \text{and} \quad \mathrm{E_{KE}} = \frac{1}{2}M_C V_p^2 \quad (23)$$

When the shear plugging stress exceeds shear plugging strength in the composite near projectile periphery, shear plugging failure occurs. Then, the energy absorbed by shear plugging can be determined:

$$\Delta E_{sp} = Nh_1 S_{sp}\pi dh \quad \text{and then} \quad E_{sp} = \sum \Delta Esp \quad (24)$$

where N is the number of layers shear plugged and S_{sp} denotes shear plugging strength.

Delamination and matrix cracking absorb a part of the initial kinetic energy of the projectile. Energies absorbed by delamination and matrix cracking at different time are given by [19]

$$\Delta E_{MCi} = P_m \pi r_{ti}^2 A_{ql} E_{mi} h V_m \text{ and } \Delta E_{DLi} = P_d \pi r_{ti}^2 A_{ql} G_{\mathrm{IIcd}} \tag{25}$$

The factors P_d and P_m stand for percentage delamination and percentage matrix cracking. Total absorbed energy by matrix cracking and delamination mechanisms are given by

$$E_{MC} = \sum \Delta E_{MCi} \qquad and \qquad E_{DL} = \sum \Delta E_{DLi} \tag{26}$$

Therefore, the total absorbed energy by laminated composite back-up plate is

$$E_{\mathrm{tot}} = \mathrm{E_{pri}} + \mathrm{E_{sec}} + \mathrm{E_{KE}} + \mathrm{E_{SP}} + \mathrm{E_{MC}} + \mathrm{E_{DL}} \tag{27}$$

Based on the energy conservation equation, during perforation, if the total absorbed energy by back-up composite and kinetic energy of the fragmented ceramic conoid equals to the kinetic energy lost by the projectile at any time t, then the failure of laminated composite has occurred.

Experimental studies

The ceramic/nanocomposite targets were fabricated using ceramic and composite laminates. In this study, alumina (Al2O3) used as faced ceramic and composite laminate comprises E-glass woven fabric and nanozirconia particles dispersed epoxy resin as back-up material. The nano-zirconia ceramic content has been chosen 5 wt%. For manufacturing ceramic/nanocomposite samples, at first, the nanocomposite laminates were fabricated in two steps. Zirconia was mixed with epoxy resin using shear mixer at 2000 r/min for 2 h and kept in the vacuum oven to remove the air bubbles, for better dispersion. The laminates of 150×150 mm were prepared by hand lay-up technique and then ceramic tile was placed on composite laminate. All ceramic tiles had in-plane dimensions of 50×50 mm. After that, compressed foam with dimension of 150×150mm with a square hole of 5050mm at its center placed and covered the laminates composites as shown in Figure 5. At the end, the prepared targets were compressed in a compression molding machine. Three nominal thicknesses (5, 8, and 10 mm) of ceramic tiles and two nominal thicknesses (3 and 5 mm) of nanocomposite panels were used in this study. The 2-mm-thick composite laminate comprises 14 plies and the 5-mmthick consists of 24 plies. For non-penetration tests, ceramic/nanocomposite panels are mounted unclamped against a back face deformation indicating colored clay block (Figure 5). In cases that the panels are not fully perforated, the ballistic performance of the panels is assessed by the shape and depth of back face signature.

In these tests, projectiles have a cylindrical shape with 10mm in diameter and 15mm height. The material of the projectile is VCN200 steel. This material is chosen to minimize the deformation of the projectile during impact. The weight of the projectile is about 9.2 g.

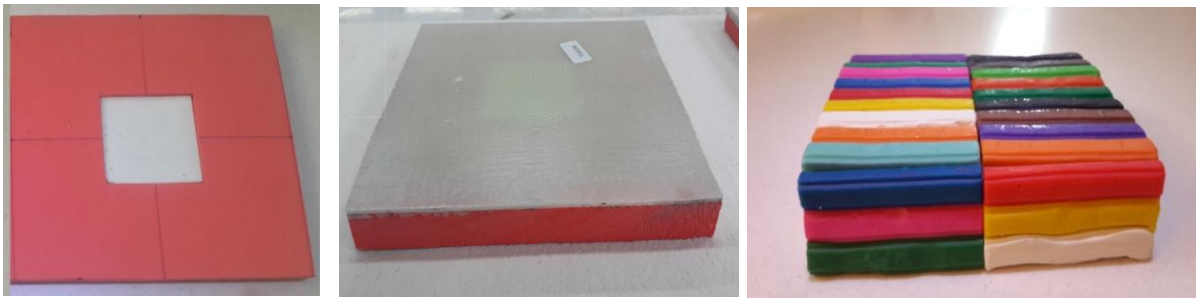

Figure 5. Ceramic/composite target, front view (left), back surface (center) and backing colored clay block (right).

Ballistic tests were performed using a gas gun test at TMU laboratory. The helium was used as gas in the chamber of the gun and its pressure was varied to get different velocities. The impact velocity is measured by light sources and photodiodes connected to a data logger.

Result and discussion

The validity of the model is assessed using the results of the experimental tests carried out in this study and other studies. Also the results of the theoretical model are compared with those from Wilkins [33] and Hetherington and Rajagopalan [34] experimental and Kang and Cho [35] and Naik et al. [10] theoretical models. Specification and mechanical properties of ceramic and composite backing plate were taken from the literature. [34] Experimental researches were carried out by Hetherington and Rajagopalan [34] on the ballistic impact performance of the typical ceramic/composite armors. The results are presented in Table 1.

Table 1. Comparison of the residual velocity obtained with new analytical model with experimental and analytical model of Naik et al. [10]

Specimen code	Ceramic thickness (mm)	Composite back up (mm)	Impact velocity (m/s)	Residual velocity (m/s)		
				Experimental [34]	Naik model [10]	New model
1	4	5	893	832	850.6	849
2	4	8	882	826	819.5	836
3	4	10	881	802	799.4	827
4	6	5	880	800	818.3	796
5	6	8	893	802	810.7	809
6	6	10	878	760	775	794
7	9	5	898	693	793.8	758
8	9	8	880	658	753.7	740
9	9	10	889	621	735.4	742
10	18	5	895	425	453.7	387
11	18	8	888	329	400.9	336
12	18	10	876	299	336.5	321

Hetherington and Rajagopalan [34] used different combinations of thicknesses of ceramic plate and composite backing plate. They used cylindrical projectiles. Projectile diameter was 12.7 mm, and projectile mass was 46.8 g. Target thickness varied from 9 to 28 mm. The nominal incident ballistic impact velocity was 886 m/s. They presented the corresponding residual velocities of the projectile.

Analytical prediction of the residual velocity and ballistic limit velocity is also presented in Table 1 and compared with results of Naik et al.'s [10] model. There is a good match between the experimental results and the analytical predictions.

Figure 6 shows the results of ballistic limit in comparison with the experimental results obtained by Wilkins. [33] In these tests, AD85 ceramic/glass FRP composite armors are used. Projectiles used in these experiments [35] are steel with 7.62mm diameter and 8.12 g mass. Other specification and mechanical properties of ceramic and FRP composite were taken from Wilkins. [33] Figure 6 shows the analytical (Kang and Cho [35] and new model) and experimental results of ballistic limit as a function of the thickness of the ceramic with the backing thickness of $t_b = 4.06$ mm.

As shown in Figure 6, there is a good agreement between new analytical model and experimental results of Wilkins. [33] As shown in this figure, the prediction of ballistic limit by the new analytical model is better than Kang analytical model. [35]

Ballistic experiment results

In this section, the trauma of back-up material of specimens was calculated by the analytical model and compared with results of experiments carried out in this study. In Table 2, the effect of ceramic thickness on trauma was presented with experimental results and compared with the prediction of the analytical model. The backing composite thickness is t_b=2 mm. As the thickness of the ceramic increases, the trauma back face decreases. There is a good agreement between the experimental results and the analytical predictions. Figure 7 shows the trauma of back-up composite created in colored clay block.

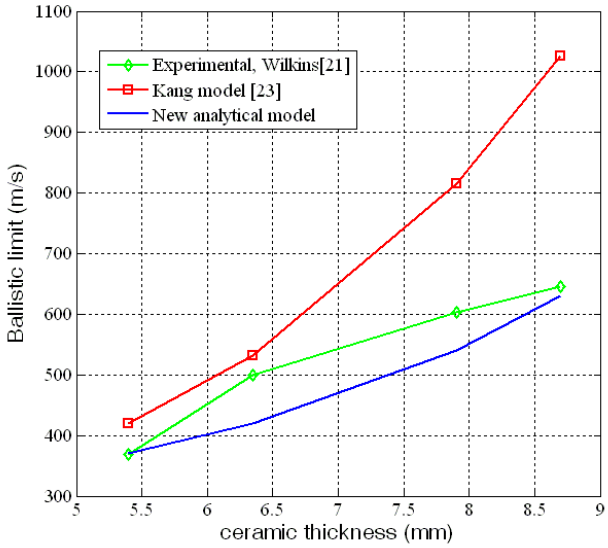

Figure 6. Analytical and experimental results of ballistic limit velocity of the target AD85/FRP composite.

The effect of impact velocity of projectile on trauma of back-up material was investigated in the experimental tests. Experimental results and analytical prediction of trauma of back-up plate at impact velocities of 190–310 m/s are presented in Table 3. It is found that the increase in impact velocity leads to the increase in back face signature value which is shown in Figure 8. The damage and failure of ceramic layer in several impact velocities are shown in Figure 9. The formation of a large central cone crack as well as radial and tangential cracks in the Al2O3 tiles after impact was observed. As shown in Figure 9, at low-impact velocities (190 m/s), only radial cracks were observed in the ceramic target progressing to include circumferential cracks with increasing velocity. At higher impact velocity, the fragment size in the ejected material is smaller with a more uniform distribution.

Table 2. Comparison of experimental and new analytical backing trauma.

serial number	Impact Velocity m/s	Ceramic Thickness mm	Composite Thickness mm	Backing trauma (mm)	
				Experimental carried in this work	New analytical model
T0524-13	310	5	5	perforated	74.5
T0824-14	310	8	5	60	65.7
T1024-15	310	10	5	31	29.6

Figure 7. Front and back view of created trauma in colored clay back up the composite at impact velocities of 190m/s and ceramic thickness (a) 10 mm and (b) 5 mm.

Effect of hardness on ballistic impact behavior

One of the most important parameters for determining the ballistic performance of ceramic composites is the ceramic hardness. The effect of ceramic hardness on the ballistic performance is studied by using two types of ceramics, AD85 and B4C, with different hardness in the same impact scenario. According to the present model, if the energy of projectile is high enough so that the ceramic is eroded, the resistance penetration is more when B4C is used. But when the energy of projectile is low enough so that the ceramic is not eroded, there will be little difference between the ballistic limit of the two ceramics AD85 and B4C.

Table 3. Comparison of experimental and new analytical backing trauma.

Serial number	Impact velocity m/s	Ceramic thickness mm	Composite thickness mm	Backing trauma (mm)	
				Experimental carried in this work	New analytical model
T1015-03	190	10	2	15	10.5
T1015-08	260	10	2	24	21.2
T1015N-06	288	10	2	29	26.1

Figure 8. Front and back view of deformation and cone formed at the colored clay of back up composite in the same target thickness and impact velocity: (a) 190m/s and (b) 310 m/s.

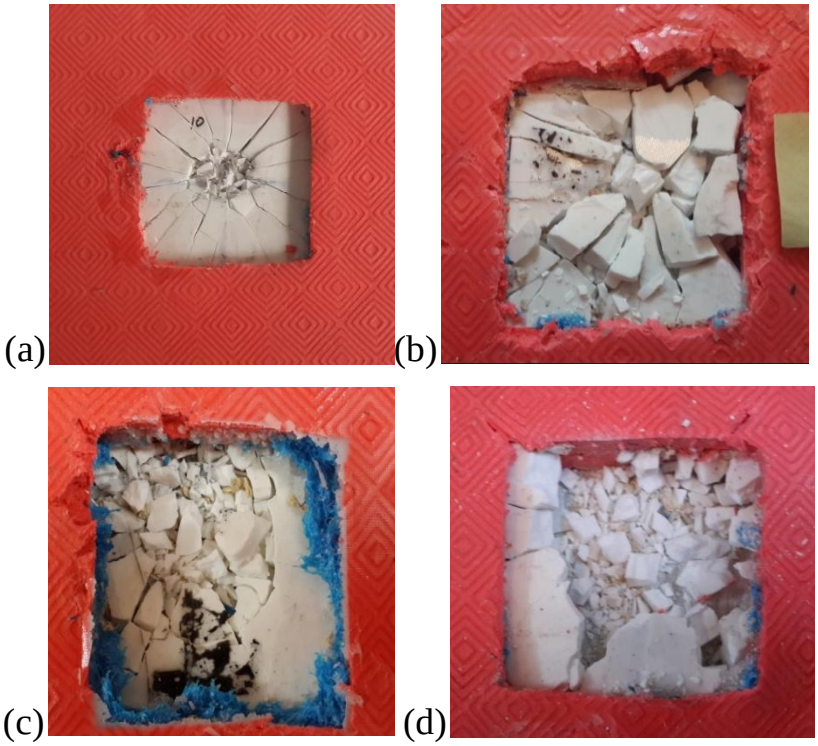

Figure 9. Comparison of ceramic fragmentation and the pattern of formed cracks after impact for impact velocities: (a) 190 m/s, (b) 260 m/s, (c) 288 m/s and (d) 310 m/s.

Figure 10 shows that when the ballistic limit velocity increases due to increase in backing thickness, the difference between the behaviors of two types of ceramic will be more pronounced.

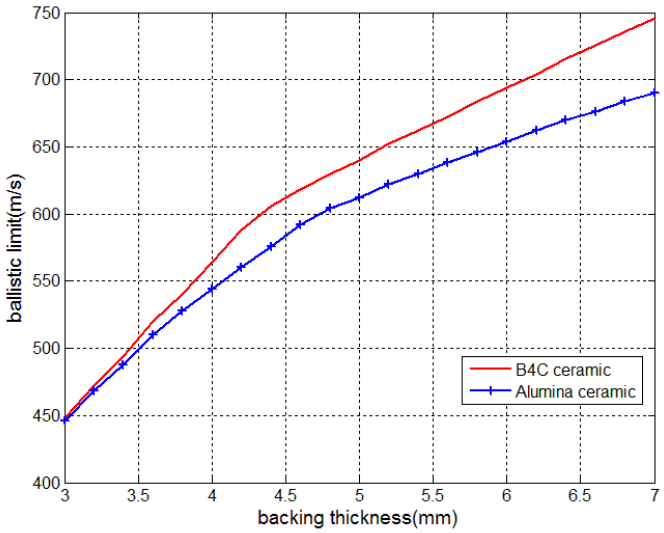

Figure 10. Effect of hardness of ceramic on ballistic limit.

The effect of nano particle of zirconia on ballistic performance

Dispersion of nano inclusions in the matrix is a very important parameter in the mechanical behavior of nanocomposites. In this section, the results of the effect of nano-zircoia

incorporation in the back-up material in the ceramic/nanocomposite target are presented. For this purpose, ballistic tests were performed on several specimens with 5wt% nano-zirconia (ZrO2) in composite back up the ceramic layer and the back face signature and width of transverse deformation were measured (by measuring dimensions of clay block). In Table 4, back face signature and width of transverse deformation were compared in three sets with and without nano-zirconia. In all specimens without nano, trauma of back face is more than trauma in specimens with nanoparticles. In fact when the back surface signature criteria were analyzed, all samples with no perforation had trauma smaller than the samples without nanoparticles. On the other hand, the addition of nanoparticles can change the failure modes. These can be translated into an increase in the delamination process and damage area. Figure 11 shows the damage area of back-up laminates of 2mm thickness and ceramic thickness of 5, 8, and 10 mm, with and without nano-zirconiain particles, respectively

This shows that the presence of nano-zirconiain composite decreases the damage area in back-up laminates. In fact during high-velocity impact, when the ballistic cone (ceramic and composite) is formed, in addition to the local compressive loading, a bending stress is also applied, mainly in the projectile impact surrounding areas. As can be observed in Figure 11, in all cases three distinct damaged zones were noticed on the back surface after impact. The first zone is a central fiber breakage region, while the second one is a much intense delamination area surrounding the fiber breakage/perforation region. The outer zone is a large region with diffuse delamination, i.e. formation of micro void and micro crack at the interface between plies.

Ballistic properties and damage mechanisms of the composites are strongly dependent on the fracture toughness and bending properties of the back-up composite including elastic modulus, tensile strength, and failure strain of fiber and matrix as well as interfacial bonding between them. Due to increase in bending strength and stiffness caused by the addition of nanozirconia particles, less delamination and matrix cracking occur and a decrease in damage area as well as an increase in absorption capability and ballistic limit of FRP composites was observed.

Table 4. Backing trauma and damage area in back up composite with and without nano zirconia.

Serial Number	Type	Impact velocity (m/s)	Trauma (mm)	Perforation	Damage Area mm^2
T0515-11	without nano	288	40	YES	2400
T0515N-12	with nano	288	40	YES	2500
T0815-09	without nano	260	38	NO	3300
T0815N-10	with nano	260	33	NO	2100
T1015-08	without nano	260	25	NO	1900
T1015N-07	with nano	260	24	NO	750

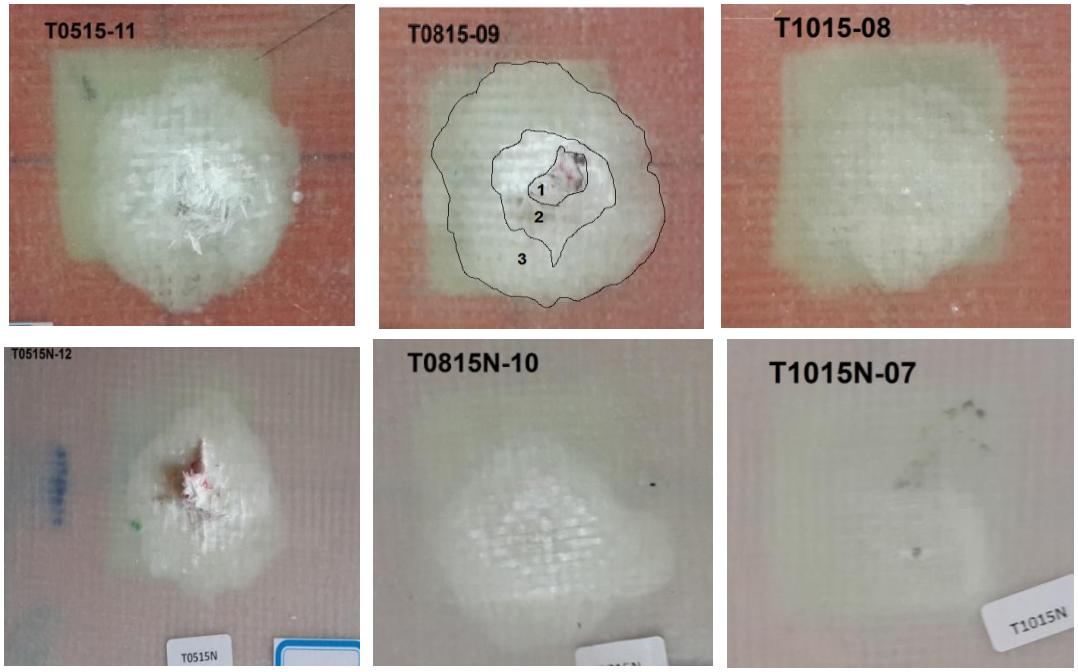

(a) (b) (c)

Figure 11. Comparison of damage area and delamination of composite laminate back up ceramic in two states, with nano and without nano at three ceramic thickness: (a) 5 mm, (b) 8 mm, and (c) 10 mm.

Conclusion

The analytical model presented in this paper is a simple and reliable way for predicting the penetration resistance of the ceramic/composite targets. It has been shown that the results of this model are in good agreement with experimental data and the results from other analytical models.

The following conclusions are made from the impact studies of the ceramic/composite targets:

- The penetration resistance of the ceramic is determined based on the dynamic cavity expansion analysis, and this led to more accurate results which are in agreement with experimental data.
- Ceramic penetration strength is intensely lowered after impact and fragmentation. Thus, ceramic penetration resistance is not constant and decreases during penetration of projectile into ceramic.
- If impact energy is high enough that leads to erosion of ceramic, then the hardness of ceramic has more influence on ballistic limit relative to the case when ceramic has no erosion.
- The addition of nanoparticles of zirconia ceramic in the glass/epoxy composite improved the ballistic impact performance in the ceramic/nanocomposite targets.
- Delamination area is controlled due to dispersion of nano-zirconia in the matrix and leads to less damaged area on the back-up composite.

Declaration of Conflicting Interests

The author(s) declared no potential conflicts of interest with respect to the research, authorship, and/or publication of this article.

Funding

The author(s) received no financial support for the research, authorship, and/or publication of this article.

References

1. Chen YL, Chu CK, Chuang WY, et al. A study of ceramic composite materials for bullet-proof optimization by using Taguchi method. In: 16th international conference on composite materials, 2007. http://www.iccm-central.org/Proceedings/ICCM16proceedings/contents/pdf/ThuH/ThHA2-02ge_chuck223209p.pdf
2. Bandaru AK, Vetiyatil L and Ahmad S. The effect of hybridization on the ballistic impact behavior of hybrid composite armors. Compos B Eng 2015; 76: 300–319.
3. Zhang XF and Li YC. On the comparison of the ballistic performance of 10% zirconia toughened alumina and 95% alumina ceramic target. Mater Des 2010; 31: 1945–1952.
4. Liu W, Chen Z, Cheng X, et al. Design and ballistic penetration of the ceramic composite armor. Compos B Eng 2016; 84: 33–40.
5. Florence A. Part II: interaction of projectiles and composite armor. Menlo Park, CA: Stanford Research Institute, 1969.
6. Woodward RL. A simple one dimensional approach to modeling ceramic composite armor defeat. Int J Impact Eng 1990; 9: 455–474.
7. Chocron Benloulo IS and Sanchez-Galvez V. A new analytical model simulate impact on to ceramic/composite Armors. Int J Impact Eng 1998; 2: 461–471.
8. Zeara R and Sanches-Galvez V. Analytical modeling of normal and oblique ballistic impact on ceramic/metal light weight armors. Int J Impact Eng 1998; 21: 133–148.
9. Tate A. A theory for the deceleration of long rods after impact. J Mech Phys Solids 1967; 15: 387–399.
10. Naik NK, Kumar S, Ratnaveer D, et al. An energy-based model for ballistic impact analysis of ceramic-composite armors. Int J Damage Mech 2012; 22: 145–187.
11. Liaghat GH, Shanazari H, Aboutorabi A, et al. A modified analytical model for analysis of perforation of projectile into ceramic composite targets. Int J Compos Mater 2013; 3: 17–22.
12. Feli S, Yas MH and Asgari MR. An analytical model for perforation of ceramic/multi-layer planer woven fabric target by blunt projectiles. Compos Struct 2011; 93:548–556.
13. Feli S and Asgari MR. Finite element simulation of ceramic/composite armor under ballistic impact. Compos B Eng 2011; 42: 771–780.

14. Liu W, Chen Z, Chen Z, et al. Influence of different back laminate layers on ballistic performance of ceramic composite armor. Mater Design 2015; 87: 421–427.

15. Krishnan K, Sockalingama S, Bansala S, et al. Numerical simulation of ceramic composite armor subjected to ballistic impact. Compos B 2010; 41: 583–593.

16. Cheeseman BA and Bogetti TA. Ballistic impact into fabric and compliant composite laminates. Compos Struct 2003; 61: 161–173.

17. Talib AA, Abbud L, Ali A, et al. Ballistic impact performance of Kevlar-29 and Al2O3 powder/epoxy targets under high velocity impact. Mater Design 2012; 35:12–19.

18. Shaktivesh NN, Kumar CS and Naik N. Ballistic impact performance of composite targets. Mater Design 2013; 51:833–846.

19. Naik NK, Shrirao P and Reddy BCK. Ballistic impact behavior of woven fabric composites: formulation. Int J Impact Eng 2006; 32: 1521–1552.

20. Wen HM. Penetration and perforation of thick FRP laminates. Compos Sci Technol 2001; 61: 1163–1172.

21. Mohan S and Velu S. Ballistic impact behavior of unidirectional fiber reinforced composites. Int J Impact Eng 2014; 63: 164–176.

22. Chen X, Zhu F and Wells G. An analytical model for ballistic impact on textile based body armor. Compos B 2013; 45: 1508–1514.

23. Shanazari H, Liaghat GH, Hadavinia H, et al. Analytical investigation of high-velocity impact on hybrid unidirectional/woven composite panels. J Thermoplast Compos Mater, Epub ahead of print 16 September 2015. DOI:DOI: 10.1177/0892705715604680.

24. Den Reijer P. Impact on ceramic faced armor. PhD thesis, Delft University of Technology, Netherlands, 1991.

25. Ning J and Ren H. Dynamic response of alumina ceramics impacted by long tungsten projectile. Int J Impact Eng 2013; 62: 60–74.

26. Satapathy S and Bless S. Calculation of penetration resistance of brittle materials using spherical cavity expansion analysis. Mech Mater 1996; 23: 323–330.

27. Feli S, Aalami Aaleagha ME and Ahmadi Z. A new analytical of normal penetration of projectile into the lightweight ceramic target. Int J Impact Eng 2010; 37:561–567.

28. Wilson D and Hetherington JG. Analysis of ballistic impact on ceramic faced armor using high speed photography. In: Proceedings of the lightweight armour system symposium, 1995. Cranfield: Royal Military College of Science.

29. Fellows NA and Bartan PC. Development of impact model for ceramic faced semi-infinite armor. Int J Impact Eng 1999; 22: 793–811.

30. Chen C, Zhu X, Hou H, et al. Analytical model for highvelocity perforation of moderately thick ultra-high molecular weight polyethylene-woven laminated plates. J Compos Mater 2015; 49: 2119–2136.

31. Smith JC, McCrackin FL and Schiefer HF. Stress-strain relationship in yarn subjected to rapid impact loading: part V: wave propagation in long textile yarns impacted transversely. J Res Natl Bur Stand 1958; 60: 517–534.

32. Guden M, Yildirima U and Hallc IW. Guden. Effect of strain rate on the compression behavior of a woven glass fiber/SC-15 composite. Polym Test 2004; 23: 719–725.

33. Wilkins ML. Mechanics of penetration and perforation. Int J Eng Sci 1978; 16: 793–807.

34. Hetherington JG and Rajagopalan BP. An investigation into the energy absorbed during ballistic perforation of composite armors. Int J Impact Eng 1991; 11: 33–40.

35. Kang KJ and Cho KZ. An estimation of ballistic limit for ceramic-FRP composite armor. KSME J 1991; 5:140–148.

Appendix 1

Notation

Ap	section area of projectile	r_l	radial of longitudinal wave front
A_c	base area of ceramic cone	r_t	radial of transverse wave front
A_{ql}	quasi-lemniscate area reduction factor	R_t	penetration resistance of ceramic
c	ceramic longitudinal sound speed	S_{sp}	shear plugging strength
c_t	velocity of longitudinal strain wave in yarns	t_c	ceramic thickness
D_p	diameter of projectile	V	velocity of projectile
d_y	the yarn density in weft and warp directions	$\dot{u}_0(t)$	velocity of the ceramic cone
d_c	diameter of ceramic cone base	x	erosion of ceramic
E	Young's modulus of yarn	$\dot{x}$	velocity of projectile-ceramic interface
E_c	Young's modulus of ceramic	Y_p	yield stress of projectile
E_{MC}	energy absorbed by matrix cracking	Y	the compressive strength of ceramic
E_{DL}	energy absorbed by delamination	β	shape factor
E_{KE}	kinetic energy of moving cone	γ	pressure–shear coefficient
E_{mt}	energy absorbed by matrix cracking per unit volume	$\dot{\gamma}$	shear strain rate
E_{pri}	strain energy of primary yarns	θ	angle of composite cone viscosity coefficient
E_{sec}	strain energy of secondary yarns	ρ_p	projectile density
E_{tot}	total energy absorbed by composite laminate	ρ_c	ceramic density
F	force exert on back up composite	ρ_t	composite density
G_{IIcd}	critical dynamic strain energy release rate in mode II	σ_{cd}	dynamic compressive stress
h_t	back up composite thickness	σ_e	quasi-static compressive strength in the through-thickness direction of the laminate
Mp	mass of projectile	σ_f	the tensile strength of ceramic
Mpr	residual mass of projectile	τ_s	quasi-static shear strength of laminate
M_c	mass of ceramic cone	τ_d	dynamic shear strength of the laminate
M_{cb}	mass of composite cone	φ_0	semi angle of ceramic cone at initial impact
P_m	percent delaminating layers	φ	semi angle of ceramic cone during penetration
P_d	percent matrix cracking		